EBioMedicine 2 (2015) 1705–1717

Contents lists available at ScienceDirect

EBioMedicine

journal homepage: www.ebiomedicine.com

Research Article

Metabolic Catastrophe in Mice Lacking Transferrin Receptor in Muscle

Tomasa Barrientos [a], Indira Laothamatas [a], Timothy R. Koves [b,c], Erik J. Soderblom [d,e], Miles Bryan [a], M. Arthur Moseley [d], Deborah M. Muoio [a,b,c], Nancy C. Andrews [a,f,*]

[a] Department of Pharmacology and Cancer Biology, Duke University School of Medicine, Durham, NC 27710, USA
[b] Molecular Physiology Institute, Sarah W. Stedman Nutrition and Metabolism Center, Duke University, Durham, NC 27704, USA
[c] Department of Medicine, Duke University School of Medicine, Durham, NC 27710, USA
[d] Duke Proteomics and Metabolomics Shared Resource, Center for Genomic and Computational Biology, Duke University School of Medicine, Durham, NC 27710, USA
[e] Department of Cell Biology, Duke University School of Medicine, Durham, NC 27710, USA
[f] Department of Pediatrics, Duke University School of Medicine, Durham, NC 27710, USA

ARTICLE INFO

Article history:
Received 17 June 2015
Received in revised form 23 September 2015
Accepted 23 September 2015
Available online 4 October 2015

Keywords:
Iron
Skeletal muscle
Transferrin receptor
Hepcidin
Intermediary metabolism

ABSTRACT

Transferrin receptor (Tfr1) is ubiquitously expressed, but its roles in non-hematopoietic cells are incompletely understood. We used a tissue-specific conditional knockout strategy to ask whether skeletal muscle required Tfr1 for iron uptake. We found that iron assimilation via Tfr1 was critical for skeletal muscle metabolism, and that iron deficiency in muscle led to dramatic changes, not only in muscle, but also in adipose tissue and liver. Inactivation of Tfr1 incapacitated normal energy production in muscle, leading to growth arrest and a muted attempt to switch to fatty acid β oxidation, using up fat stores. Starvation signals stimulated gluconeogenesis in the liver, but amino acid substrates became limiting and hypoglycemia ensued. Surprisingly, the liver was also iron deficient, and production of the iron regulatory hormone hepcidin was depressed. Our observations reveal a complex interaction between iron homeostasis and metabolism that has implications for metabolic and iron disorders.

1. Introduction

Iron, required by all mammalian cells, circulates bound to plasma transferrin (Tf). Cells express transferrin receptor (Tfr1), which can bind Fe-Tf and internalize it by receptor-mediated endocytosis (Hentze et al., 2004). Vesicles bearing Fe-Tf/Tfr1 fuse with endosomes, where low pH releases iron from Tf for transmembrane transfer to the cytoplasm. Iron is then stored, used directly, or incorporated into heme or Fe–S clusters for utilization in globin proteins, cytochromes, oxidative phosphorylation complexes and other enzymes. Apo-Tf and Tfr1 recycle to the cell surface for further rounds of iron uptake.

Although Tfr1 is widely expressed, it is not universally required for iron assimilation. Through genetic manipulations in mice, we showed that most early embryonic tissues develop normally in the absence of Tfr1, and most adult tissues can form from $Tfr1^{-/-}$ embryonic stem cells (Levy et al., 1999; Ned et al., 2003). Furthermore, most tissues are not iron deficient in mice with a congenital deficiency of Tf, but rather accumulate excess iron (Trenor et al., 2000). However, hematopoietic cells, particularly erythroid precursors, have a critical requirement for Tfr1 (Levy et al., 1999; Ned et al., 2003) and Tf (Trenor et al., 2000). We hypothesized that non-hematopoietic cells might use alternative iron uptake mechanisms, and such mechanisms have been described (Sturrock et al., 1990; Barisani et al., 1995; Baker et al., 1998; Yang et al., 2002; Oudit et al., 2003; Liuzzi et al., 2006; Li et al., 2009). We considered that skeletal muscle is a major site of iron utilization (Andrews, 1999), and asked whether Tfr1 was important.

We found that skeletal muscle has a critical requirement for Tfr1. Mice in which the muscle *Tfr1* gene has been inactivated during embryogenesis appeared normal at birth, but rapidly developed a dramatic and lethal phenotype. They stopped growing, lost adipose tissue, developed hepatic steatosis and experienced profound hypoglycemia before death. Although Tfr1 was intact in hepatocytes, the liver also became iron deficient early in the development of the phenotype and decreased production of the iron regulatory hormone hepcidin. The abnormal phenotype was corrected by administration of parenteral iron to saturate transferrin, increasing non-Tf-bound iron, indicating that neonatal muscle iron deficiency was responsible for the severe, systemic metabolic derangement.

2. Materials and Methods

2.1. Animal Experiments

We crossed 129/SvEv mice bearing a floxed *Tfr1* (gene symbol *Tfrc*) allele (Chen et al., 2015) with B6.Cg-Tg (ACTA1-cre)79Jme/J mice

* Corresponding author at: DUMC 2927, Durham, NC 27710, USA.
E-mail address: nancy.andrews@duke.edu (N.C. Andrews).

http://dx.doi.org/10.1016/j.ebiom.2015.09.041

(Jackson Laboratory #006,149) expressing Cre recombinase under the control of the human skeletal muscle actin promoter (Miniou et al., 1999). We backcrossed with 129/SvEv mice for more than 10 generations. As indicated in the figure legends, microarray experiments and experiments shown in Fig. 1A,C,F,G,H,I, and Fig S1C used mice with similar, mixed 129/C57BL6 backgrounds and experiments shown in all other figures used mice with a homogeneous 129/SvEv background. Apart from several days' difference in length of survival, the phenotypes were very similar on both backgrounds. Animals were genotyped by PCR using genomic DNA from toe clips (Truett et al., 2000). Primers are described in Table S1. Blood glucose was measured at P6 using the FreeStyle Freedom Lite monitoring system (Abbott). Insulin levels were measured using a Rat/Mouse Insulin ELISA kit (EMD Millipore) according to the manufacturer's protocol. Total ketones were measured using a Total Ketone Bodies kit (Wako Diagnostics) according to the manufacturer's protocol. Glycogen measurements were performed as previously described (Thyfault et al., 2007). Non-heme iron was measured as previously described (Levy et al., 1999). For iron rescue experiments, mice were injected IP with 5 mg of Uniferon® 100 (25 μL) at P3, or at both P3 and P21. All procedures were carried out under protocols approved by the Duke Animal Care and Use Committee. Sample sizes included in animal protocols were determined with assistance from the Duke Biostatistics Core.

2.2. RNA Extraction, Microarray Analysis and Quantitative PCR

RNA was extracted using an RNA isolation kit (Qiagen) according to the manufacturer's instructions. Samples were treated with DNase I (Qiagen) to remove genomic DNA. Microarray analysis was performed using Affymetrix Mouse Expression Array 430A 2.0. RNA quality control, hybridization and data analysis were performed by the Duke University Microarray Shared Resource (see Supplemental Experimental Procedures) and results have been deposited in the NCBI Gene Expression Omnibus database, accession number GSE68675. For quantitative PCR, cDNA from liver and skeletal muscle was synthesized using the iScript cDNA synthesis kit (Bio-Rad) according to the manufacturer's instructions. Real time quantification was performed using iQ SYBR Green Super mix (Bio-Rad). The primer sequences are described in Table S1.

2.3. Immunoblots

Protein lysates were prepared from muscle and liver using RIPA buffer (50 nM NaCl, 20 mM Tris, pH 7.5, 1 mM EDTA,1% NP40, 0.1% SDS, 0.5% Na deoxycholate), protease inhibitors and phosphatase inhibitors (Roche Applied Science). Quantification was performed using Bio-Rad Dc Protein Assay (Bio-Rad). Lysates we subjected to electrophoresis on TGX™ precast gels (Bio-Rad) and transferred to Immune-Blot® PVDF membrane (Bio-Rad). Membranes were incubated with primary and secondary antibodies listed in Table S2, developed with chemiluminescence ECL Western blotting detection solutions (GE Healthcare) and exposed to autoradiography film (HiBlot CL®, Denville Scientific). Signal intensity was quantified using Image J software.

2.4. Morphometric analysis

Tibialis anterior (TA) muscle was isolated from mice and immediately flash frozen in embedding media. Muscle cross-sections were stained with Alexa Fluor® 594 WGA (Life Technologies, Invitrogen) and individual fibers were counted using Image J software.

2.5. Oil Red O Staining

Liver was harvested from mice and frozen in embedding media. 10 μm sections were stained with Oil Red O as previously reported (Carson and Hladlik, 2009).

2.6. IRP-IRE Binding Assay

IRP-IRE binding assays were carried out using the LightShift™ Chemiluminescent RNA EMSA according to manufacturer's instructions (Pierce Biotechnologies). The IRE sequence is shown in Table S1.

2.7. Enzymatic Assays

Aconitase activity was measured in isolated mitochondria using the Aconitase Enzyme Activity Microplate Assay Kit (Abcam) according to the manufacturer's instructions. Mitochondria were isolated as previously described (Wieckowski et al., 2009). Complex II activity was measured in gastrocnemius tissue lysates as previously reported (Spinazzi et al., 2011).

2.8. Metabolomics Analyses

Amino acids, acylcarnitines and organic acids were analyzed using stable isotope dilution techniques. Amino acids and acylcarnitine measurements were made by flow injection tandem mass spectrometry as described previously (An et al., 2004; Wu et al., 2004). The data were acquired using a Waters Acquity™ UPLC system equipped with a triple quadrupole detector and a data system controlled by MassLynx 4.1 operating system (Waters). Organic acids were quantified using methods described previously (Jensen et al., 2006) employing Trace Ultra GC coupled to ISQ MS operating under Xcalibur 2.2 (Thermo Fisher Scientific).

2.9. Proteomics Analyses

Proteomics analysis on 6 gastrocnemius samples was carried out by the Duke Proteomics and Metabolomics Shared Resource (see Supplemental Experimental Procedures). Proteomics results have been deposited in the MassIVE database (https://massive.ucsd.edu/ProteoSAFe/static/massive.jsp), ID MSV000079328.

2.10. Statistical Analyses

Unpaired Student's T tests were performed using Microsoft ® Excel® 2011 software. *P* values less than 0.05 were considered significant. Representation of the *p* values are as follows: not significant (ns), $p > 0.05$, $^{*}p \le 0.05$, $^{**}\ p \le 0.01$, $^{***}\ p \le 0.001$, $^{****}\ p \le 0.0001$.

3. Results

3.1. Tfr1 Deficiency in Skeletal Muscle Causes early Postnatal Death

We selectively inactivated the murine *Tfr1* gene using a skeletal muscle actin (HSA)-Cre transgene, expressed from embryonic day 9 and highly specific for skeletal muscle (Miniou et al., 1999), to recombine loxP sites flanking *Tfr1* exons 3 to 6 (Chen et al., 2015) to generate $Tfr1^{mu/mu}$ mice. $Tfr1^{mu/mu}$ mice were born in Mendelian ratios. We confirmed that they expressed little Tfr1 mRNA or protein in skeletal muscle (Fig S1). They were slightly smaller than $Tfr1^{fl/fl}$ wild type (WT) littermates at birth, fell behind in growth (Fig. 1A,B) and typically died or had to be euthanized before P13 on a mixed background or P11 on a homogeneous 129/SvEv background. Because the males usually lived longer and therefore had larger tissues, we continued our analysis with male mice unless otherwise noted. Necropsy revealed that the $Tfr1^{mu/mu}$ mice had small muscles (Fig. 1C,D) but the total number

of fibers was preserved (Fig. 1E). We did not observe degenerative changes such as central nuclei or misalignment of Z-lines but we saw lipid droplets in diaphragmatic muscle by electron microscopy (not shown).

We found striking changes in other tissues, even though Tfr1 was targeted only in muscle. Fat pads were present early in life in Tfr1$^{mu/mu}$ mice (not shown) but disappeared by the time animals showed distress (Fig. 1F). Before growth delay was apparent the abdominal organs appeared grossly normal (not shown), but later the Tfr1$^{mu/mu}$ liver contained excess neutral lipid and both liver and spleen were small compared to controls (Fig. 1G–I). Although normal at day 4 (not shown), serum glucose became low as the phenotype developed (Fig. 1J). At P6 serum insulin ranged from 0.5 to 6.7 ng/mL in control animals (n = 18) but was undetectable in almost all mutants (n = 17). Two mutant animals that did have measurable serum insulin (1.3 and 1.5 ng/mL) also had normal serum glucose (117 and 94 mg/dL respectively), suggesting that they had not yet developed the full phenotype. Low serum glucose, coupled with non-detectable serum insulin, would exacerbate the glucose deficit in insulin-responsive tissues – muscle and fat – likely contributing to the phenotype. Serum ketones were elevated at P6 in both control and mutant animals, consistent with their young age, but markedly more elevated in the mutants (Fig. 1K). Surprisingly, liver glycogen was indistinguishable between controls and mutants, but muscle glycogen was decreased in Tfr1$^{mu/mu}$ mice (Fig. S1D). The animals may have succumbed to hypoglycemia, but attempts to rescue the animals by administering intraperitoneal glucose did not substantially prolong survival (not shown). Alternatively, they may have died from respiratory failure due to diaphragmatic insufficiency. We speculate that normal placental function spared the mice before birth, when serum glucose levels are maintained by the mother (Wang et al., 1995) and that changes developed when the animals no longer benefited from the placenta's capacity to correct metabolic abnormalities and substrates for gluconeogenesis decreased, as described later.

3.2. Muscle Iron Deficiency and Impaired Oxidative Phosphorylation

We asked whether skeletal muscle was iron deficient in the absence of Tfr1. In mice with homogeneous 129 backgrounds and earlier onset of the phenotype, the total amount of muscle iron, per gram of tissue, was similar between Tfr1$^{mu/mu}$ mice and controls at P6 as measured by inductively coupled plasma mass spectrometry (not shown). However, muscle ferritin was decreased (Fig. 2A,B) and iron regulatory protein binding activity was increased in Tfr1$^{mu/mu}$ animals at P6 (Fig. 2C,D), indicative of iron deficiency. Myoglobin was decreased, consistent with insufficiency of its co-factor heme (Fig S2A,B). This suggests that the animals had a normal endowment of iron at birth, but additional iron was not assimilated for muscle growth and functional iron deficiency ensued.

Heme and Fe–S clusters are critical cofactors for electron transport chain (ETC) complexes and failure of mitochondrial respiration might contribute to the phenotype observed in Tfr1$^{mu/mu}$ mice. We evaluated the integrity of ETC complexes I to V at P6 by immunoblotting with a cocktail of antibodies that detects labile protein components of each. Although complex V was represented similarly in WT and Tfr1$^{mu/mu}$ mice, the mutants were deficient in the other complexes (Fig. 2E,F), which require iron (Xu et al., 2013). We confirmed complex II deficiency by enzymatic assay (Fig. 2G) and also observed that a key Fe–S containing protein of complex I, Ndufs3, was markedly decreased (Fig. 2H,I). The deficiencies in ETC complexes did not appear to result from a substantial decrease in the number of mitochondria because complex V levels (Fig. 2E) were similar in WT and Tfr1$^{mu/mu}$ mice and expression of mitochondria-encoded mRNA transcripts (Fig S2C) was not substantially different between WT and Tfr1$^{mu/mu}$ mice. These results support the interpretation that Tfr1$^{mu/mu}$ muscle was iron deficient, leading to impaired mitochondrial respiration.

3.3. *Tfr1$^{mu/mu}$* Mice are Rescued by Iron

We hypothesized that if Tfr1 is needed for iron assimilation by skeletal muscle, it might be possible to rescue the mutant phenotype by causing iron overload. We knew that muscle could take up non-Tf-bound iron in animals with a congenital deficiency of Tf (Trenor et al., 2000). We treated WT and Tfr1$^{mu/mu}$ mice with a large dose of iron dextran at P3 to increase circulating non-Tf-bound iron. With this treatment, Tfr1$^{mu/mu}$ mice appeared healthy, had normal body weights (Fig. 3A,B), survived for at least 4 weeks with no further intervention, and survived for substantially longer with a second treatment. Both WT and Tfr1$^{mu/mu}$ mice had marked tissue iron overload as expected, and the extent of iron loading was similar (Fig. 3C,D; note log scale). H-ferritin was similarly increased in mice of both genotypes (Fig. 3E,F). At 4 weeks Tfr1$^{mu/mu}$ mice had normal serum glucose levels (Fig. 3G). We conclude that iron deficiency is the root cause of the mutant phenotype, and that it can be rescued by administration of excess iron.

3.4. Decreased Liver Iron in *Tfr1$^{mu/mu}$* Mice

Hepatic steatosis and hypoglycemia indicated that muscle iron deficiency led to changes in the liver, even though the *Tfr1* gene was intact and expressed (Fig. 4A). While we observed substantial variability, likely due to variation in the onset of the abnormal phenotype, liver non-heme iron was unexpectedly decreased at P6, and H-ferritin was reduced, indicating liver iron deficiency (Fig. 4B–D). Consistent with hepatic iron deficiency, activity of the Fe–S cluster-dependent enzyme mitochondrial aconitase was decreased (Fig. 4E) and mRNA encoding the iron regulatory hormone hepcidin was markedly diminished (Fig. 4F). Decreased liver iron did not appear to be due to systemic iron deficiency because hemoglobin and hematocrits were not significantly different between P6 mutant and control mice (not shown). These results suggest that loss of Tfr1 in skeletal muscle led to hepatic iron deficiency.

3.5. Gene Expression Changes in *Tfr1$^{mu/mu}$* Muscle and Liver

We profiled mRNA expression changes in Tfr1$^{mu/mu}$ tissues relative to WT controls [results deposited online (Barrientos and Andrews, 2015)]. In this experiment we used mice on a mixed background because they lived longer and therefore had larger tissues for mRNA extraction. We analyzed muscle and liver from mice at P5 (early), before the phenotype was grossly apparent, and P9 (late), when the phenotype had developed and the animals were within several days of death. We used Gene Set Enrichment Analysis [GSEA; (Subramanian et al., 2005; Mootha et al., 2003)] to look for informative patterns. Few genes were differentially regulated in Tfr1$^{mu/mu}$ muscle early, but *Tfr1* mRNA containing non-deleted exons was upregulated, consistent with iron deficiency. Other upregulated genes included *Cacna2d1*, a subunit of a voltage-dependent calcium channel that has been implicated in non-Tf-bound iron uptake in the heart, (Oudit et al., 2003), angiopoietin-like 4 (*Angptl4*), carbonic anhydrase 2 (*Car2*) and retinol saturase (*Retsat*). The most strongly downregulated genes in early muscle included frizzled b (*Frzb*), low density lipoprotein receptor-related 2 binding protein (*Lrp2bp*), H-ras-like suppressor (*Hrasls*), growth factor receptor-bound protein 14 (*Grb14*), contactin associated protein-like 2 (*Cntnap2*) and myosin heavy chain 4 (*Myh4*).

Later, after the phenotype became apparent, more genes were differentially regulated in mutant muscle. Upregulated genes were

annotated by GSEA as associated with hypoxia,[1] Mapk signaling,[2] glycolysis[3], Ppar signaling,[4] fatty acid metabolism[5] and Tnfα signaling.[6] Predicted targets of Nfat[7] and estrogen receptor-related protein α (Esrra, also called Nr3b1)[8] were particularly prominent. The most strongly upregulated gene was ankyrin repeat domain 2 (*Ankrd2*), which has been reported to inhibit myoblast differentiation (Mohamed et al., 2013). *Angptl4* and brain-derived neurotrophic factor (*Bdnf*), both induced by fasting (Kersten et al., 2009; Walsh et al., 2015), were also upregulated. Genes downregulated in late muscle were annotated as being involved in metabolism of amino acids, heme metabolism[9] and mTorc1 signaling.[10]

We also examined hepatic gene expression. We saw many changes early, before steatosis was apparent. The most prominent categories of upregulated genes were those involved in Tnfα signaling via NF-κB,[11] apoptosis[12], hypoxia[13], lipid and lipoprotein metabolism,[14] insulin signaling,[15] PPAR signaling[16] and fatty acid, triacylglycerol and ketone metabolism.[17] The most strongly upregulated were regulator of G-protein 16 (*Rgs16*), leptin receptor (*Lepr*), oxidative stress growth inhibitor 1 (*Osgin1*), D site albumin promoter binding protein (*Dbp*) and pantothenate kinase 1 (*Pank1*). Genes downregulated in early liver included, strikingly, more than 50 genes, mostly E2F targets, which are involved in DNA replication and the cell cycle. The most strongly downregulated gene was *Hamp*, encoding the iron regulatory hormone hepcidin, consistent with Fig. 4F.

After the phenotype became apparent, at the late time point, more genes were differentially regulated in the mutant liver. Upregulated genes were annotated in GSEA as involved in TNFα signaling, metabolism of lipids and lipoproteins, insulin signaling, adipocytokine signaling, carbohydrate metabolism and lipid, fatty acid, triacylglycerol and ketone body metabolism. *Rgs16*, *Lepr* and *Pank1* were again among the most highly induced, along with G protein-coupled receptor 64 (*Gpr64*), cytochrome P450 family 2, subfamily c, polypeptide 39 (*Cyp2c39*), apolipoprotein A-IV (*Apoa4*) and thioredoxin interacting protein (*Txnip*). Transcripts encoding enzymes involved in gluconeogenesis – *Ldhb*, encoding a subunit of lactate dehydrogenase, *Pck1*, encoding phosphoenolpyruvate carboxykinase, and *G6pc*, encoding glucose-6-phosphatase – were markedly increased, as were hepatocyte nuclear factor 4 alpha (*Hnf4a*) and nuclear receptor subfamily 4, group A, member 1 (*Nr4a1*), both transcription factors that induce gluconeogenesis. Of note, Hnf4a has been reported to repress hepcidin expression (Courselaud et al., 2002). Genes downregulated in the mutant liver at the later time included many E2F target genes involved in the cell cycle, transmembrane transporters, and genes involved in heme metabolism. The most strongly downregulated genes were *Slc22a7*, *Slc22a29*, both organic anion transporters. Other members of the Slc22 family of organic anion transporters were also downregulated.

3.6. Metabolic Changes

To better understand the complex phenotype of Tfr1$^{mu/mu}$ mice, we considered molecular events that might cause arrested growth, hepatic steatosis and hypoglycemia. We examined skeletal muscle after the phenotype was grossly apparent and observed increased expression of *Bdnf* mRNA (microarray data) and increased phosphorylation of AMPK (Fig S3A), consistent with an attempt to stimulate fatty acid oxidation and glucose uptake. We also observed decreased phosphorylation of AKT, consistent with a decrease in muscle growth, and, accordingly, decreased phosphorylation of proteins downstream of the AKT target mTOR (Fig S3B–D). The ratio of Map1lc3-II (LC3-II) to LC3-I was increased, suggesting induction of autophagy (Fig S3E). All of these changes represent responses to energy insufficiency or nutrient deprivation.

To evaluate metabolic changes, we carried out a metabolomics analysis on muscle, liver and serum from WT and Tfr1$^{mu/mu}$ mice at P4 and P6 on a 129 background, before and after the phenotype was apparent, respectively (Fig. 5). All results are shown because there were qualitative and quantitative differences between the two time points, but for simplicity the P6 results, from after the phenotype had developed, will be discussed primarily.

In Tfr1$^{mu/mu}$ muscle we observed increased accumulation of three tricarboxylic acid (TCA) cycle intermediates – citrate, α-ketoglutarate, and succinate, as well as succinyl-carnitine (C4-DC), which derives from succinyl-CoA – and decreased amounts of fumarate and malate. These changes may be attributable to decreased activity of aconitase and succinate dehydrogenase enzymes, which both require Fe–S cluster co-factors. We also saw progressive elevation of C4OH (3-OH butyryl carnitine) suggesting increasing ketone delivery to or ketolysis within the mutant muscle. Odd chain acylcarnitines (C5OH, C5:1, C3DC) were increased, consistent with increased amino acid catabolism and diminished amino acids detected in muscle. Increased branched chain amino acids (leucine, isoleucine) probably contributed to the increase in C5OH. Some β oxidation intermediates were slightly increased, but interestingly not to levels typically observed during starvation or exercise. Tfr1$^{mu/mu}$ muscle showed diminished anaplerotic amino acids, consistent with increased amino acid catabolism in an attempt to fuel the TCA cycle. Aspartic acid, one of the anaplerotic amino acids, is also used for several transamination reactions. Importantly, there were decreased levels of lactate and alanine, both precursors for gluconeogenesis that are typically shuttled from muscle to liver during starvation and exercise.

We observed increased muscle citrate, usually a signal of plenty, which can inhibit phosphofructokinase and glycolysis and may inhibit β oxidation indirectly. At the same time, impaired oxidative phosphorylation may lead to an increased AMP/ATP ratio and activation of AMPK (Fig S3A), which is a signal of energy insufficiency. In addition to these mixed signals, we observed increased acetylcarnitine (C2), which derives from acetyl CoA and might reflect mitochondrial accumulation of this crucial metabolite.

The livers of Tfr1$^{mu/mu}$ mice should stabilize serum glucose through gluconeogenesis but the mice became hypoglycemic towards the end of the first week of life. A previous report linked hepatocyte iron deficiency to decreased gluconeogenesis in an in vitro system (Klempa et al., 1989) but in our animals changes in the metabolomics profile suggested that amino acid insufficiency was the reason for failure of gluconeogenesis. Amounts of almost all amino acids were severely decreased in serum at P6. Hepatic citrate was markedly elevated, in spite of metabolic stress, possibly because diminished liver iron caused decreased mitochondrial aconitase activity (Fig. 4E). In contrast to muscle, where beta-oxidation may have been impaired due to ETC deficiencies, there was a strong signature for hepatic fatty acid catabolism, with markedly elevated even chain acylcarnitines.

Serum from Tfr1$^{mu/mu}$ mice was also more severely affected at P6 than P4. The older mice had increased C4OH suggesting increased ketone delivery or ketolysis in tissues such as muscle and heart. There

[1] *Bnip3*, *Cdkn1a*, *Irs2*, *Maff*, *Nfil3*, *Klf6*, *Fos*, *Pnrc1*, *Foxo3*, *Pim1*, *Angptl4*, *Ctgf*, *Mxi1*, *Errfi1*
[2] *Fos*, *Nr4a1*, *Hspa1a*, *Hspa1b*, *Bdnf*
[3] Irs2, Angptl4, Fbp2, Egln3
[4] *Angptl4*, *Ctgf*, *Anrd1*, *Pdpk1*, *Acsl1*, *Slc27a1*, *Fabp3*
[5] *Ca2*, *Acsl1*, *Retsat*, *Hadhb*, *Etfdh*, *Acss1*, *Eci2*
[6] *Cdkn1a*, *Irs2*, *Maff*, *Nfil3*, *Klf6*, *Fos*, *Pnrc1*, *Nr4a1*, *Nfkbi1*, *Gadd45b*, *Klf10*
[7] *Bdnf*, *Nr4a1*, *Fos*, *Ctgf*, *Csrp3*, *Cdkn1a*, *Pdk4*, *Acss1*, *Irs2*
[8] *Bdnf*, *Csrp3*, *Cdkn1a*, *Pnrc1*, *Insr*, *Errfi1*, *Tnfrsf12a*, *Abtb2*, *Gna13*, *Arhgap24*, *Asxl1*, *Golga4*, *Fabp3*, *Pim1*, *Hspb7*, *Nfil3*, *Etfdh*, *Tln1*, *Bnip3*, *Ca2*, *Fam69b*
[9] *E2f2*, *Pc*, *Alas2*, *Fam46c*, *Spta1*, *Snca*, *Slc25a37*
[10] *Sqle*, *Ctsc*, *Igfbp5*, *Tmem97*, *Ldlr*, *Me1*, *Slc37a4*, *Glrx*, *Psat1*, *Serp1*
[11] *Per1*, *Klf10*, *Bmp2*, *Nfkbia*, *Eif1*, *Jun.*, *Nr4a1*, *Maff*, *Ppap2b*, *Sgk1*, *Irs2*, *Cebpb*, *Zfp36*, *Gadd45b*, *Zbtb10*, *Nr4a2*, *Btg2*, *Nfe2l2*, *Klf9*, *Tiparp*, *Clcf1*
[12] *Jun.*, *Bmp2*, *Btg2*, *Gadd45b*, *Retsat*, *App*, *Txnip*, *Tnfrsf12a*, *Erbb3*, *Bcl2l11*, *H1f0*, *Gstm1*
[13] *Jun.*, *Irs2*, *Maff*, *Zfp36*, *Tiparp*, *Angptl4*, *Pck1*, *Errfi1*, *Egfr*, *Nedd4l*, *Upg2*, *Slc37a4*
[14] *Ppap2b*, *Angptl4*, *Trib3*, *Lpin2*, *Acox1*, *Abcc3*, *Lpin1*, *Chka*, *Chkb*, *Cpt1a*, *Cyp7b1*, *Me1*, *Nr1d1*, *Lss*, *Pnpla2*
[15] *Irs2*, *Pck1*, *G6pc*, *Eif4ebp1*, *Cblb*, *Cblc*, *Insr*, *Gys2*
[16] *Angptl4*, *Pck1*, *Acox1*, *Cpt1a*, *Me1*, *Nr1d1*
[17] *Angptl4*, *Trib3*, *Chka*, *Lss*, *Atf5*

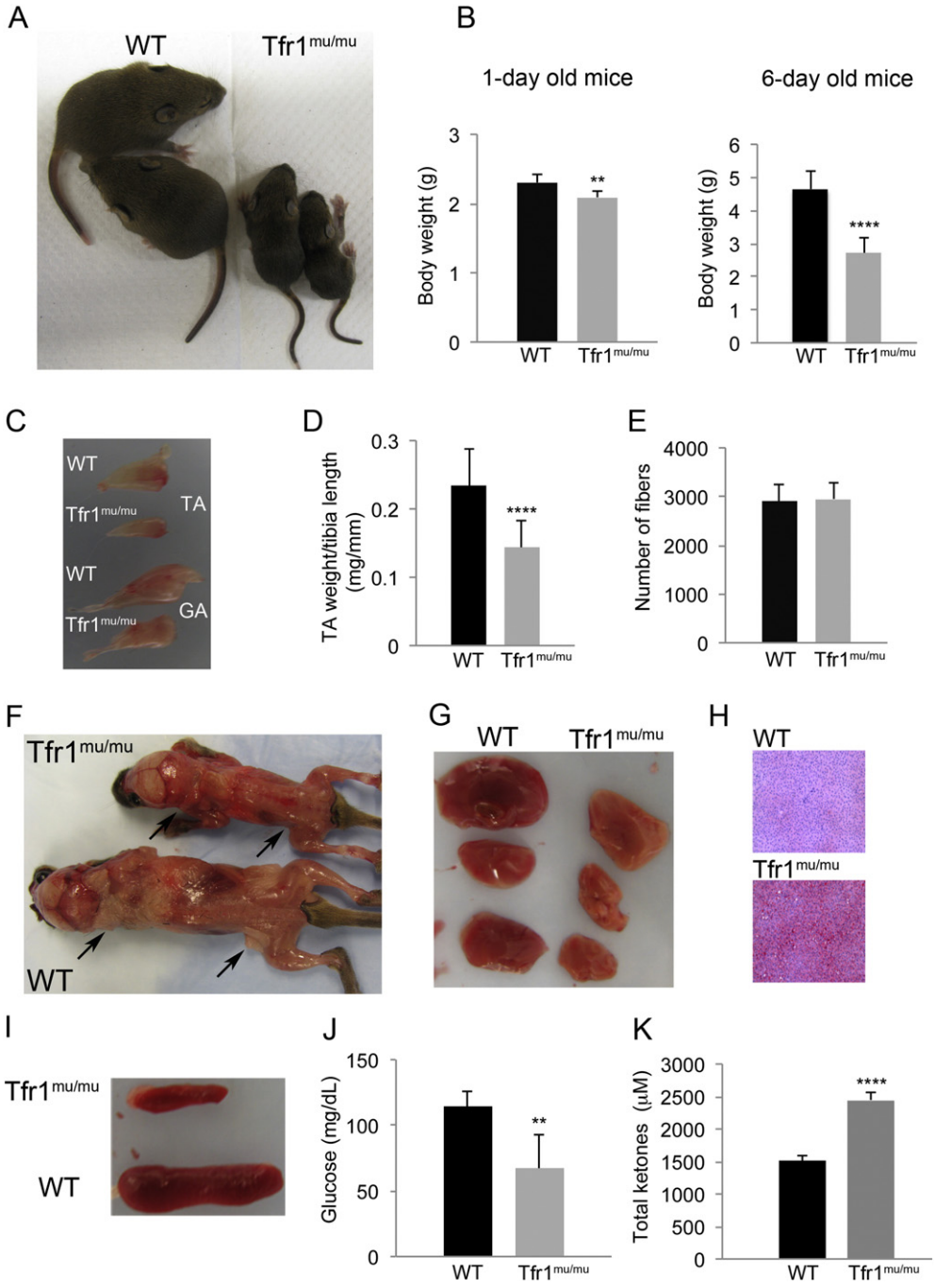

Fig. 1. Phenotypic characterization of Tfr1$^{mu/mu}$ mice. (A) Appearance of WT and Tfr1$^{mu/mu}$ mice at P9 (C57/129 mixed background). (B) Body weights at P1 (WT n = 7, Tfr1$^{mu/mu}$ n = 7; 129 background), and P6 (WT n = 5, Tfr1$^{mu/mu}$ n = 10; 129 background). (C) Tibialis anterior (TA) and gastrocnemius (GA) muscles from P9 WT and Tfr1$^{mu/mu}$ mice (C57/129 mixed background). (D) Ratio of tibialis anterior (TA) mass to tibia length at P6 (WT n = 25, Tfr1$^{mu/mu}$ n = 27; 129 background). (E) Tibialis anterior fiber numbers in Tfr1$^{mu/mu}$ and WT mice at P6 (WT n = 5, Tfr1$^{mu/mu}$ n = 4; 129 background). (F) P9 Tfr1$^{mu/mu}$ mice lacked body fat pads found in control mice, as indicated with arrows (C57/129 mixed background). (G) Gross morphology of P9 WT and Tfr1$^{mu/mu}$ livers (WT n = 3, Tfr1$^{mu/mu}$ n = 3; C57/129 mixed background). (H) Oil Red O staining (red) of liver sections (C57/129 mixed background). (I) Gross morphology of spleens at P9 (C57/129 mixed background). (J) Serum glucose measurements at P6 (male mice; WT n = 5, Tfr1$^{mu/mu}$ n = 10; 129 background). (K) Serum ketone measurements at P6 (male mice; WT n = 12, Tfr1$^{mu/mu}$ n = 12; 129 background). For all panels with graphs: Error bars represent standard deviation, ** p ≤ 0.01, **** p ≤ 0.0001.

was a robust increase in several long chain acylcarnitines derived from long chain acyl-CoA intermediates of β oxidation. As noted earlier, all amino acids were strongly diminished, likely contributing to the failure of gluconeogenesis.

3.7. Proteomic Analysis

To further evaluate the phenotype, we subjected muscle proteins from P6 (late) WT and Tfr1$^{mu/mu}$ mice to mass spectrometry-based proteomic analysis. We assessed relative protein expression levels and lysine acetylation modifications (data online at https://massive.ucsd.edu/ProteoSAFe/static/massive.jsp, ID MSV000079328). The relative expression levels of most proteins were not different between WT and mutant muscle samples. However, consistent with mRNA profiling results, the amounts of myosin heavy chain 4 (Myh4) and eukaryotic translation elongation factor 1 alpha 2 (Eef1a2) were strongly diminished and the amount of acetyl-coA acyltransferase 2 (Acaa2) was increased (Fig. 6A). The most striking changes were in proteins that

did not show altered mRNA expression: components of ETC complexes I (Ndufa5, 6, 9, 10; Ndufb9; Ndufs1, 3, 4, 5, 7, and Ndufv1), II (Sdha, Sdhb), and cytochrome C were all depleted in mutant mice compared to WT animals (Fig. 6A). Each of these complexes and many of these proteins use Fe–S clusters or heme as co-factors. Others have reported decreased expression of ETC proteins in iron deficient muscle (Rensvold et al., 2013) and noted that mRNA and protein levels did not always correlate. Decreased ETC proteins may reflect instability of their complexes when iron is insufficient.

We examined the acetyl-proteome of P6 Tfr1$^{mu/mu}$ muscle by isolating lysine-acetylated peptides using an anti-acetyl lysine antibody followed by mass spectrometry analysis (Fig. 6B, Table S3). Strikingly, nearly all proteins with increased acetylation in the mutant were mitochondrial. Multiple subunits of complex V, which do not contain iron and were not diminished in total protein levels, were hyperacetylated. Furthermore, nearly every enzyme of the TCA cycle was multiply hyperacetylated. The only exception was succinate dehydrogenase, an iron-containing enzyme shared with oxidative phosphorylation. As

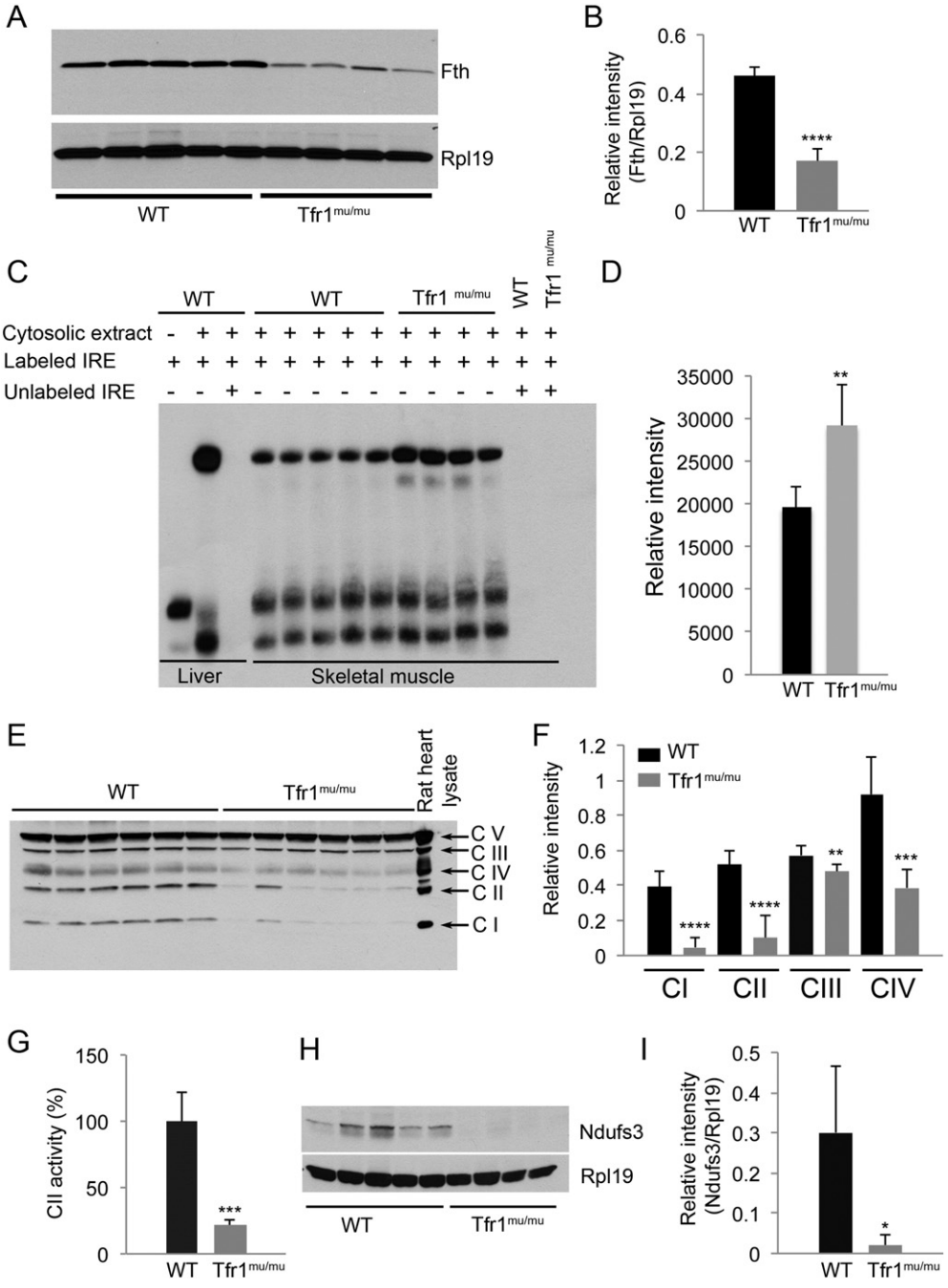

Fig. 2. Skeletal muscles with deletion of Tfr1 have decreased iron levels. (A,B) H-ferritin (Fth) levels in P6 Tfr1$^{mu/mu}$ muscle compared to WT littermates [ribosome protein L19 (Rpl19) loading control; WT n = 5, Tfr1$^{mu/mu}$ n = 4; 129 background]. (C,D) Iron regulatory protein (IRP) binding to a biotinylated iron regulatory element (IRE) probe in P6 Tfr1$^{mu/mu}$ muscle compared to WT (WT n = 5, Tfr1$^{mu/mu}$ n = 4; 129 background). (E,F) Levels of representative proteins for complexes I (Ndufb8), II (Sdhb), III (Uqcrc2), and IV (Mtco1) in muscle from P6 Tfr1$^{mu/mu}$ mice compared to WT. The amount of ATP5A, a protein component of complex V, appeared unchanged and was used in panel F to normalize for relative intensity (WT n = 6, Tfr1$^{mu/mu}$ n = 6; 129 background). (G) Enzymatic activity of Complex II in P6 Tfr1$^{mu/mu}$ muscle compared to WT (WT n = 5, Tfr1$^{mu/mu}$ n = 3; 129 background). (H,I) Fe–S containing protein Ndufs3 in P6 muscle from Tfr1$^{mu/mu}$ mice [ribosome protein L19 (Rpl19) loading control; WT n = 5, Tfr1$^{mu/mu}$ n = 4; 129 background]. All panels: error bars represent standard deviation; * p ≤ 0.05, ** p ≤ 0.01, ***p ≤ 0.001, ****p ≤ 0.0001.

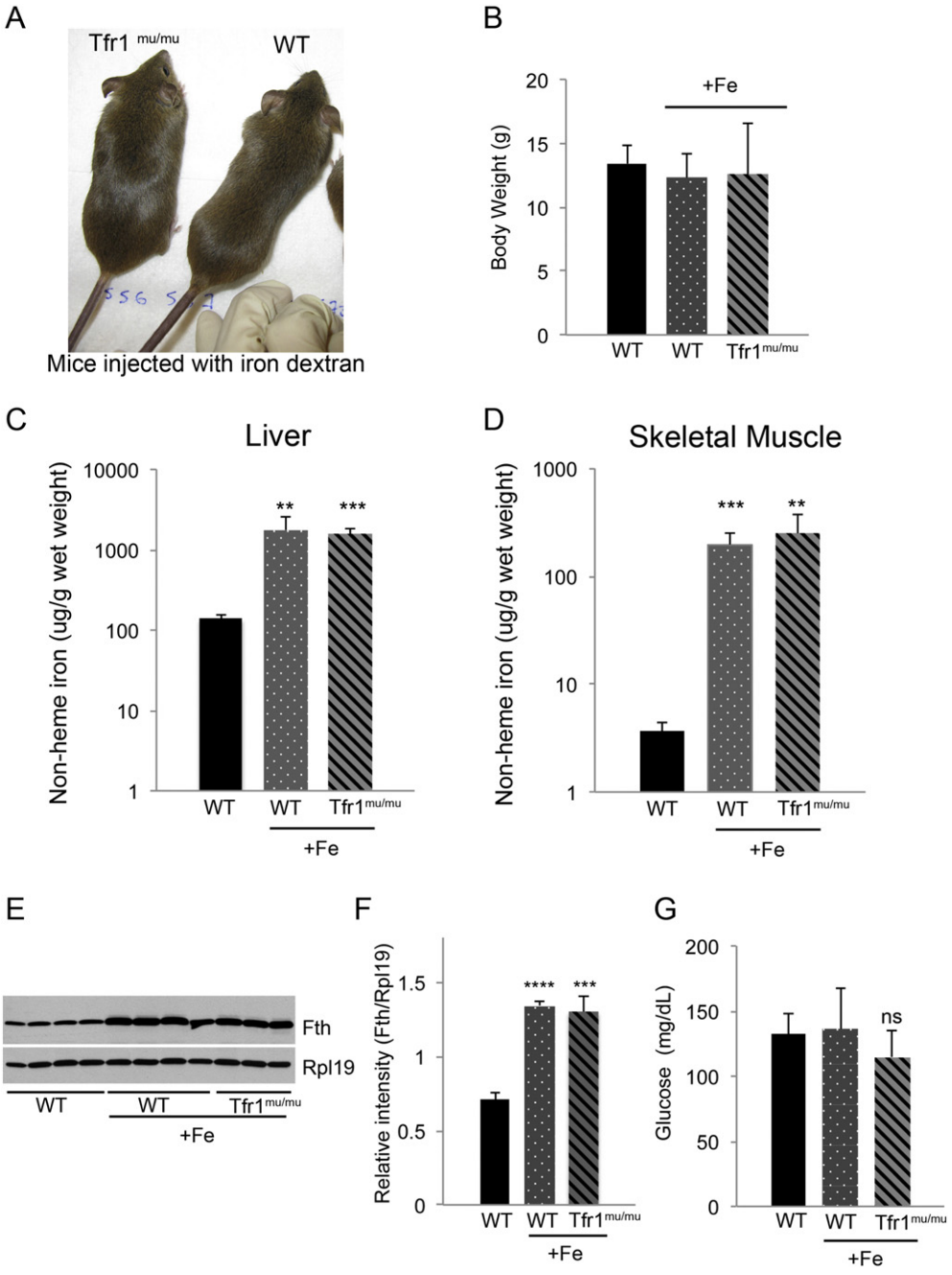

Fig. 3. Exogenous iron rescues the Tfr1$^{mu/mu}$ phenotype. (A) Representative adult Tfr1$^{mu/mu}$ and WT mice treated with iron dextran. (B) Body weights of untreated WT and iron dextran treated WT and Tfr1$^{mu/mu}$ mice. + Fe indicates iron treatment (untreated WT n = 4, treated WT n = 4, treated Tfr1$^{mu/mu}$ n = 3). (C) Non-heme liver iron in WT and Tfr1$^{mu/mu}$ mice treated with iron. + Fe indicates mice treated with iron (note Log10 scale; untreated WT n = 4, treated WT n = 4, treated Tfr1$^{mu/mu}$ n = 3). (D) Non-heme skeletal muscle iron in WT and Tfr1$^{mu/mu}$ mice treated with iron. + Fe indicates mice treated with iron (note Log10 scale; untreated WT n = 4, treated WT n = 4, treated Tfr1$^{mu/mu}$ n = 3). (E,F) Muscle H-ferritin (Fth) in WT and Tfr1$^{mu/mu}$ mice treated with iron. + Fe indicates mice treated with iron [ribosome protein L19 (Rpl19) loading control; untreated WT n = 4, treated WT n = 4, treated Tfr1$^{mu/mu}$ n = 3]. (G) Blood glucose levels in WT and Tfr1$^{mu/mu}$ mice treated with iron. + Fe indicates mice treated with iron (untreated WT n = 4, treated WT n = 4, treated Tfr1$^{mu/mu}$ n = 3). Differences in blood glucose were not significant. For all panels: mice are one-month old females on a 129 background. Error bars represent standard deviation; ns = no significant, ** p ≤ 0.01, ***p ≤ 0.001, ****p ≤ 0.0001.

mentioned earlier, amounts of Sdha and Sdhb were diminished, likely resulting in decreased activity of that enzyme.

Mitochondrial aconitase, Aco2, was the most highly hyperacetylated protein in Tfr1$^{mu/mu}$ muscle (Table S3). While it was hyperacetylated on multiple residues, acetylation on K245 was markedly increased relative to control muscle. K245 would be buried within the protein and inaccessible in its native conformation (Dick Brennan, Duke Biochemistry, personal communication). Furthermore, acetylation of K245, if it occurred before protein folding, would disrupt the normal conformation. As mentioned earlier, Aco2 contains an Fe–S cluster, which may be limiting in iron-deficient cells. We speculate that, similar to what has been shown with Aco1 (Walden et al., 2006), unavailability of the Fe–S cluster may result in a dramatic conformational change in Aco2, making K245 accessible for acetylation. This would be consistent with the increase in muscle citrate we observed (Fig. 5).

Acetylation of TCA cycle enzymes has been reported (Anderson and Hirschey, 2012) but its consequences are not well understood. If

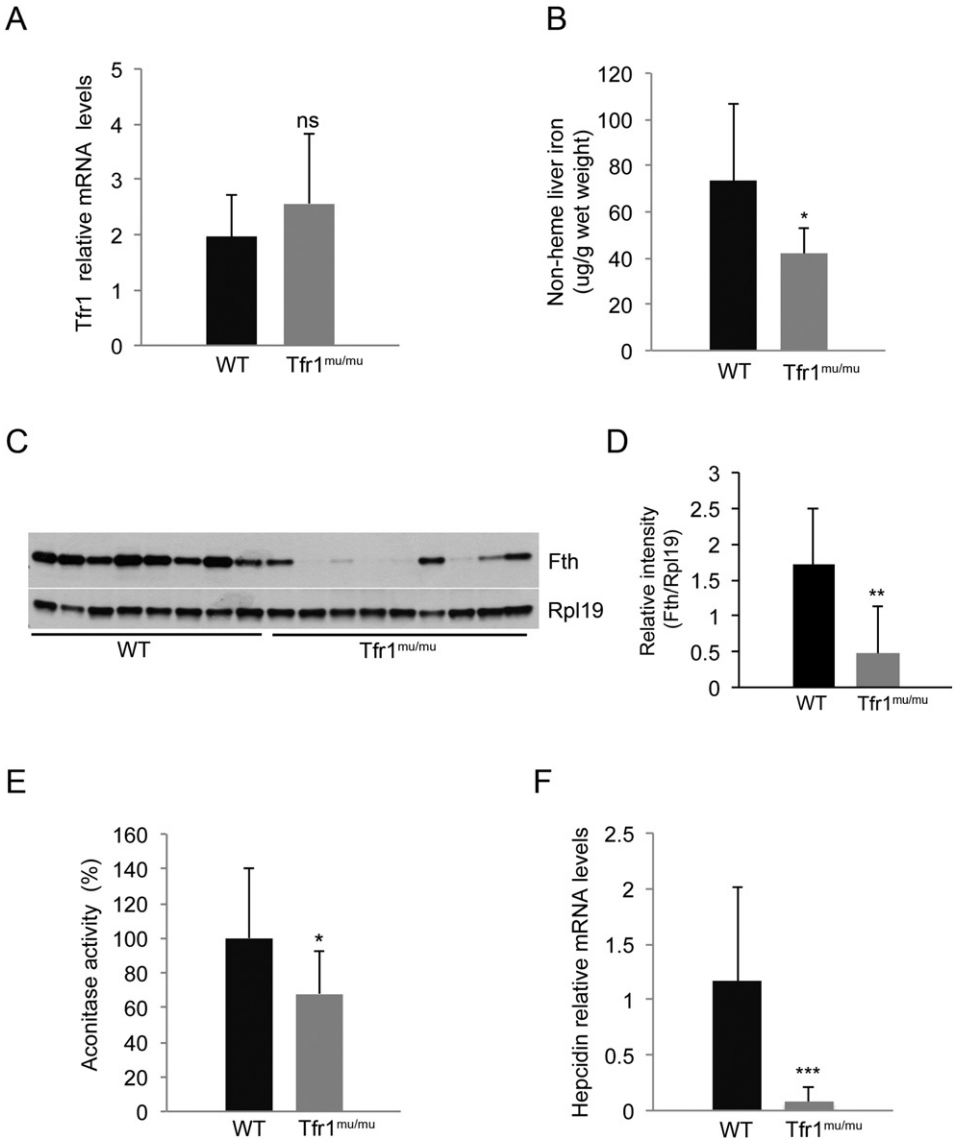

Fig. 4. Hepatic iron is decreased in Tfr1$^{mu/mu}$ mice. (A) Relative Tfr1 mRNA levels in livers from P6 WT and Tfr1$^{mu/mu}$ mice (WT n = 10, Tfr1$^{mu/mu}$ n = 11; 129 background). (B) Non-heme liver iron in P6 WT and Tfr1$^{mu/mu}$ mice (WT n = 8, Tfr1$^{mu/mu}$ n = 8, 129 background). (C,D) Liver H-ferritin (Fth) in WT and Tfr1$^{mu/mu}$ mice [ribosome protein L19 (Rpl19) loading control; WT n = 8 and Tfr1$^{mu/mu}$ n = 9; 129 background]. (E) Aconitase activity in liver from P6 WT and Tfr1$^{mu/mu}$ mice (WT n = 10, Tfr1$^{mu/mu}$ n = 12; 129 background). (F) Relative hepcidin mRNA levels in liver from P6 WT and Tfr1$^{mu/mu}$ mice (WT n = 10, Tfr1$^{mu/mu}$ n = 11; 129 background). Error bars represent standard deviation; ns = no significant, * p ≤ 0.05, ** p ≤ 0.01, *** p ≤ 0.001.

acetylation activates the enzymes, it might represent an attempt to increase the activity of the TCA cycle. However, in the absence of a functional ETC, this would be ineffective. Furthermore, it appears that the pyruvate dehydrogenase complex may be inactive, causing a switch away from the TCA cycle by inhibiting conversion of pyruvate to acetyl CoA. We observed increased acetylation of K321 of pyruvate dehydrogenase alpha 1 (Pdha1) (Table S3), which decreases its activity (Ozden et al., 2014), and increased phosphorylation of S293 (Fig S3F), which has the same effect (Rardin et al., 2009). The phosphorylation of S293 may be carried out by pyruvate dehydrogenase kinase isoenzyme 4 (Pdk4) and *Pdk4* mRNA was markedly increased in our microarray profiles.

Interestingly, many enzymes important for β oxidation were also hyperacetylated (Fig. 6B, Table S3). Acetylation of these proteins has been described in normal heart (Foster et al., 2013) and other cell types (Kim et al., 2006) but for the most part the functional consequences have not been determined. Lysine acetylation of long chain acyl-CoA dehydrogenase (Acadl) on two specific residues was shown to inhibit activity (Bharathi et al., 2013), but neither of those residues was hyperacetylated in our mutant muscle samples.

Increased mitochondrial acetyl CoA might drive enzymatic or non-enzymatic acetylation of mitochondrial proteins. Furthermore, decreased NAD levels, predicted due to impairment of complex I activity, could contribute to hyperacetylation by inhibiting sirtuin deacetylase activity. We noted that many of the acetylation events we observed corresponded to previously described targets of sirtuin 3 (Sirt3), a mitochondrial deacetylase (Rardin et al., 2013). Although we did not attempt to measure Sirt3 activity directly, it is likely impaired, contributing to the metabolic defects. We compared our results to results from Sirt3 −/− muscle proteomic analysis (CR Kahn, B Gibson, M Rardin personal communication of unpublished results) and found that, of a total of 349 hyperacetylated peptides in Tfr1$^{mu/mu}$ muscle and 397 hyperacetylated peptides in Sirt3 −/− muscle, there were 70 peptides common to both datasets that changed in the same direction (Table S4).

4. Discussion

We found that Tfr1 is important in murine skeletal muscle, and that iron deficiency consequent to the loss of Tfr1 set off a chain of events that resulted in systemic metabolic abnormalities and early postnatal lethality. Tfr1$^{mu/mu}$ mice appeared normal at birth and had normal numbers of skeletal muscle fibers, making it unlikely that they suffered a developmental defect. Furthermore, there was no evidence of muscle atrophy or necrosis. However, over the first week of life the mutant animals stopped growing, lost body fat, developed hepatic steatosis and became incapable of maintaining normal serum glucose levels, with death ensuing before the end of the second week. This dramatic

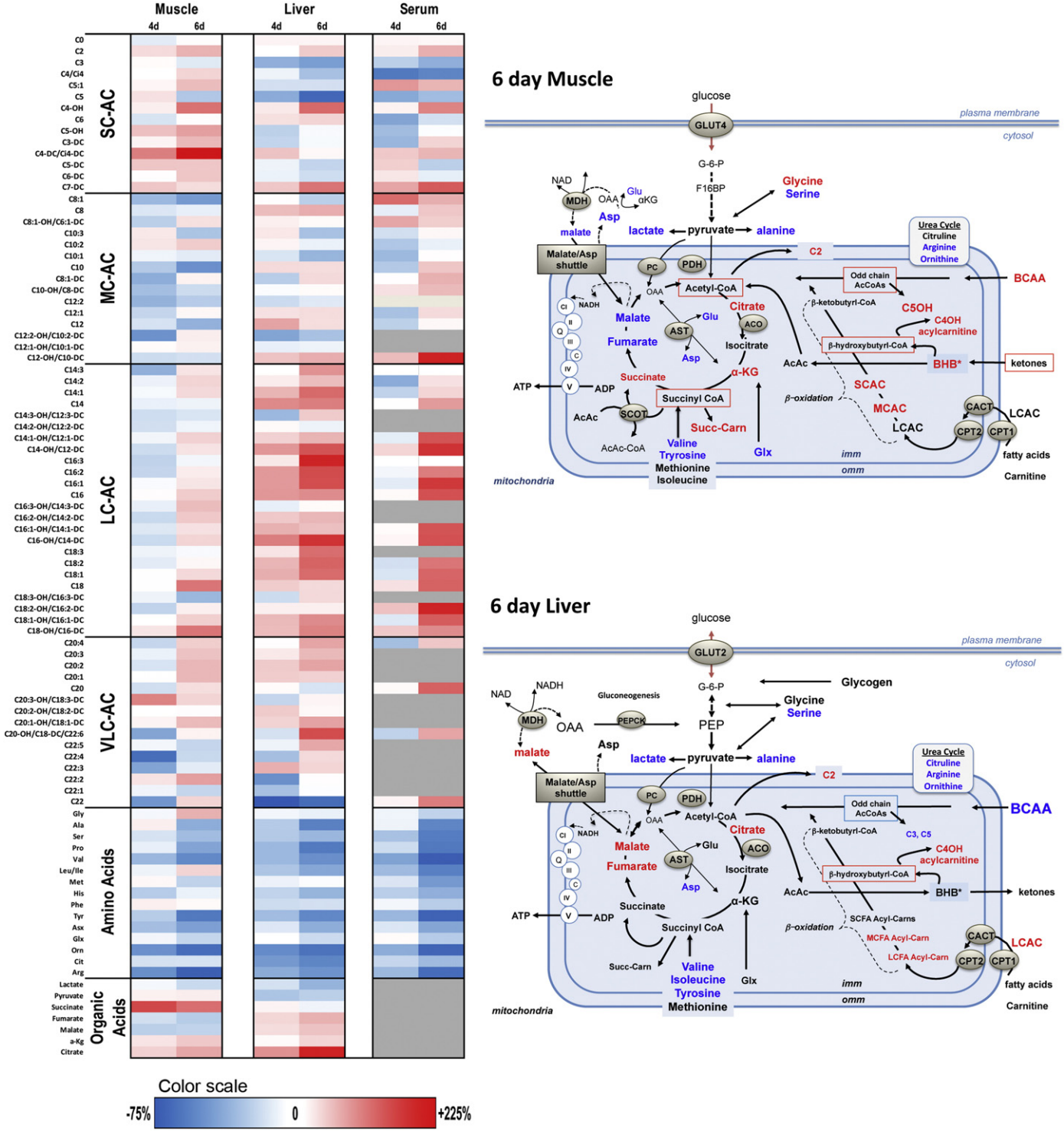

Fig. 5. Metabolic changes in Tfr1$^{mu/mu}$ mice. (Left panel) Heat map of metabolomics results from gastrocnemius muscle, liver and serum from P4 (4d) and P6 (6d) WT and Tfr1$^{mu/mu}$ mice (males; 129 background). Blue — decreased, red — increased, white — not significantly different from WT, gray — not determined; SC — short chain, MC — medium chain, LC — long chain, VLC — very long chain, AC — acylcarnitine. Because the animals were small, we pooled tissue from 3 to 4 mice for each sample in this analysis. At P4 we analyzed 6 pools each for WT and Tfr1$^{mu/mu}$ (total 23 mice of each genotype). At P6 we analyzed 6 pools each for WT and Tfr1$^{mu/mu}$ (total 18 mice of each genotype). P4 Tfr1$^{mu/mu}$ mice were compared to P4 WT mice and P6 Tfr1$^{mu/mu}$ mice were compared to P6 WT mice. (Right panels) Diagrammatic representation of pathways changing in the muscle (top) and liver (bottom) of Tfr1$^{mu/mu}$ mice. Metabolites highlighted in blue are decreased and metabolites highlighted in red are increased.

A

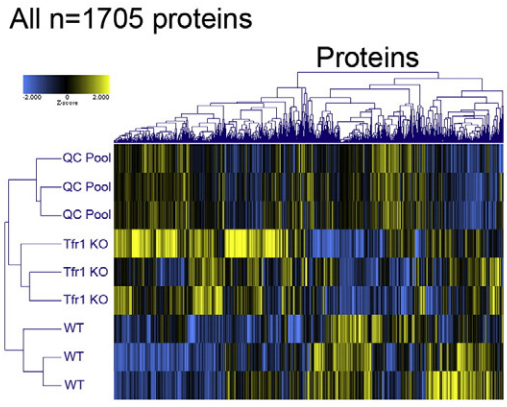

Protein Name	Gene Name	Protein Description	Peptides per Proteins	fold-change ($Tfr1^{mu/mu}$ vs WT)	FDR Correct Ttest P-value
SDHB	Sdhb	Succinate dehydrogenase [ubiquinone] iron-sulfur subunit, mitochondrial	3	-4.6	0.048
NDUS1	Ndufs1	NADH-ubiquinone oxidoreductase 75 kDa subunit, mitochondrial	15	-4.1	0.020
NDUA5	Ndufa5	NADH dehydrogenase [ubiquinone] 1 alpha subcomplex subunit 5	3	-3.8	0.028
NDUS4	Ndufs4	NADH dehydrogenase [ubiquinone] iron-sulfur protein 4, mitochondrial	2	-3.8	0.019
NDUV1	Ndufv1	NADH dehydrogenase [ubiquinone] flavoprotein 1, mitochondrial	11	-3.8	0.019
NDUA6	Ndufa6	NADH dehydrogenase [ubiquinone] 1 alpha subcomplex subunit 6	2	-3.7	0.045
NDUAA	Ndufa10	NADH dehydrogenase [ubiquinone] 1 alpha subcomplex subunit 10, mitochondrial	8	-3.4	0.020
NDUS3	Ndufs3	NADH dehydrogenase [ubiquinone] iron-sulfur protein 3, mitochondrial	5	-3.4	0.019
EF1A2	Eef1a2	Elongation factor 1-alpha 2	6	-3.2	0.025
NDUS5	Ndufs5	NADH dehydrogenase [ubiquinone] iron-sulfur protein 5	4	-3.1	0.020
NDUS7	Ndufs7	NADH dehydrogenase [ubiquinone] iron-sulfur protein 7, mitochondrial	2	-2.9	0.048
MYH4	Myh4	Myosin-4	84	-2.9	0.019
SDHA	Sdha	Succinate dehydrogenase [ubiquinone] flavoprotein subunit, mitochondrial	11	-2.7	0.020
NDUA9	Ndufa9	NADH dehydrogenase [ubiquinone] 1 alpha subcomplex subunit 9, mitochondrial	5	-2.7	0.019
CYC	Cycs	Cytochrome c, somatic	5	-2.0	0.049
NDUB9	Ndufb9	NADH dehydrogenase [ubiquinone] 1 beta subcomplex subunit 9	2	-2.0	0.020
MYPC2	Mybpc2	Myosin-binding protein C, fast-type isoform 2	31	-1.8	0.020
F136A	Fam136a	Protein FAM136A	2	1.5	0.019
THIM	Acaa2	3-ketoacyl-CoA thiolase,	17	1.5	0.048
GPC4	Gpc4	Glypican-4	3	1.7	0.026
MPPB	Pmpcb	Mitochondrial-processing peptidase subunit beta	2	2.4	0.025

B

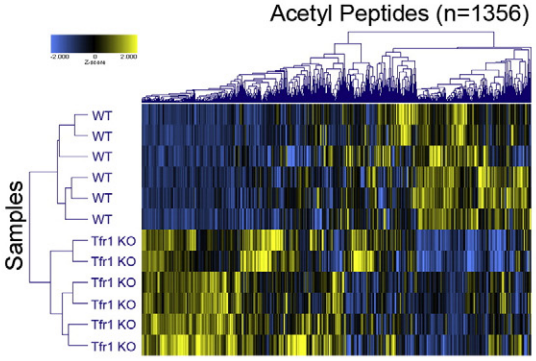

Proteins components of complex V

Protein Name	Gene Name	Protein Description
ATPA	Atp5a1	ATP synthase subunit alpha, mitochondrial
ATPB	Atp5b	ATP synthase subunit beta, mitochondrial
ATPD	Atp5d	ATP synthase subunit delta, mitochondrial
AT5F1	Atp5f1	ATP synthase subunit b, mitochondrial
ATP5H	Atp5h	ATP synthase subunit d, mitochondrial
ATP5J	Atp5j	ATP synthase-coupling factor 6, mitochondrial
ATP5L	Atp5l	ATP synthase subunit g, mitochondrial

Proteins components of TCA cycle

Protein Name	Gene Name	Protein Description
ACON	Aco2	aconitate hydratase, mitochondrial
IDHP	Idh2	isocitrate dehydrogenase [NADP], mitochondrial
IDH3A	Idh3a	isocitrate dehydrogenase [NAD] subunit alpha, mitochondrial
IDH3B	Idh3b	isocitrate dehydrogenase 3, beta subunit
IDHG1E	Idh3g	isocitrate dehydrogenase [NAD] subunit gamma 1, mitochondrial
ODO1	Ogdh	2-oxoglutarate dehydrogenase, mitochondrial isoform 2
DLDH	Dld	dihydrolipoyl dehydrogenase, mitochondrial
SUCA	Suclg1	succinyl-CoA ligase [ADP/GDP-forming] subunit alpha, mitochondrial
SUCB1	Sucla2	succinyl-CoA ligase [ADP-forming] subunit beta, mitochondrial
FUMH	Fh1	fumarate hydratase, mitochondrial
MDHM	Mdh2	malate dehydrogenase, mitochondrial
CISY	Cs	citrate synthase, mitochondrial

PDH complex

Protein Name	Gene Name	Protein Description
ODPA	Pdha1	pyruvate dehydrogenase E1 component subunit alpha, somatic form, mitochondrial

Proteins involved in β oxidation

Protein Name	Gene Name	Protein Description
CPT2	Cpt2	carnitine O-palmitoyltransferase 2, mitochondrial
ACADS	Acads	short-chain specific acyl-CoA dehydrogenase, mitochondrial
ACADM	Acadm	medium-chain specific acyl-CoA dehydrogenase, mitochondrial
ACADL	Acadl	long-chain specific acyl-CoA dehydrogenase, mitochondrial
ACADV	Acadvl	very long-chain specific acyl-CoA dehydrogenase, mitochondrial
HCDH	Hadh	hydroxyacyl-coenzyme A dehydrogenase, mitochondrial
ECHA	Hadha	trifunctional enzyme subunit alpha, mitochondrial
ECHB	Hadhb	trifunctional enzyme subunit beta, mitochondrial
ETFA	Etfa	electron transfer flavoprotein subunit alpha, mitochondrial
ETFB	Etfb	electron transfer flavoprotein subunit beta
ECI1	Eci1	enoyl-CoA delta isomerase 1, mitochondrial
THIM	Acaa2	3-ketoacyl-CoA thiolase, mitochondrial

Fig. 6. Proteomic analysis shows increased acetylation in proteins in muscle of $Tfr1^{mu/mu}$ mice. (A) Heat map showing the global protein expression of three pools of $Tfr1^{mu/mu}$ gastrocnemius (9–10 mice per pool) and three pools of WT gastrocnemius (7 mice per pool) at P6 (males; 129 background). The table lists proteins with significant changes in expression in $Tfr1^{mu/mu}$ mice compared to WT mice. (B) Heat map of acetyl proteome of three $Tfr1^{mu/mu}$ and three WT mice at 6 days of age. We used the same pooled samples as in (A). The table lists proteins with significant increase in acetylation in $Tfr1^{mu/mu}$ mice compared to WT mice.

phenotype was fully reversed by administration of high dose iron dextran, showing that muscle iron deficiency was the root cause.

Ineffective iron assimilation, due to loss of Tfr1, disrupted muscle metabolism. Representative proteins from iron-containing ETC complexes I to IV were decreased and enzymatic assay confirmed that complex II activity was impaired in skeletal muscle when the phenotype was apparent. Complex V subunits and TCA cycle enzymes were hyperacetylated. While the consequences of hyperacetylation are uncertain for most of these enzymes, in one case we can infer a functional outcome. Aco2, the mitochondrial aconitase involved in the TCA cycle, was highly acetylated on a lysine residue that is not normally exposed. Its accessibility indicates that Aco2 was acetylated when it was not properly folded, likely because of unavailability of Fe–S clusters due to iron deficiency, consistent with the decreased Aco2 activity and accumulation of citrate in muscle. Increased Pdk4 expression and specific acetylation and phosphorylation events affecting Pdha1 likely

inhibited the pyruvate dehydrogenase complex in skeletal muscle, precluding conversion of pyruvate to acetyl CoA. This may have caused a switch to attempted use of β-oxidation of fatty acids and/or ketones in muscle. However, we can only infer the metabolic consequences, because we have not done comprehensive metabolic flux experiments, which would be very difficult in newborn mice.

Metabolic changes were not limited to skeletal muscle, although Tfr1 was only deficient in that tissue. Body fat pads disappeared, suggesting that lipolysis ensued, presumably to provide a source of energy for muscle, and the liver became steatotic. Tfr1-null muscle showed increased expression of *Angptl4* mRNA, suggesting a starvation-like response. Starvation should promote lipolysis for increased fatty acid delivery to the muscle, but failure of the ETC would preclude effective β oxidation. We do not know why the levels of acylcarnitines were lower in muscle than liver, but this might suggest a defect in muscle fatty acid uptake or in the activity of carnitine palmitoyltransferase 1 (Cpt1). The presence of lipid droplets in the diaphragm was consistent with increased fatty acid delivery and decreased β oxidation. *Angptl4* expression has also been associated with hypoglycemia, inhibition of gluconeogenesis and hepatic steatosis (Xu et al., 2005), as observed in our mice.

There was evidence that the liver was attempting to respond by increasing gluconeogenesis to provide glucose for muscle metabolism. Several mRNAs that encode proteins inducing gluconeogenesis were increased in the liver, including *Rgs16* (Pashkov et al., 2011), *Pank1* (Leonardi et al., 2010) and *Txnip* (Muoio, 2007). Lactate dehydrogenase b (*Ldhb*) was markedly induced, suggesting that the liver was trying to use lactate to produce pyruvate through the Cori cycle. Transcripts encoding phosphoenolpyruvate carboxykinase (*Pck1*) and the catalytic subunit of glucose-6-phosphatase (*G6pc*) were also increased. We note that expression of *Pck1* and *G6pc* is controlled by Rev.-erbα (Nr1d1), a transcription factor that binds heme, and heme binding is reported to repress *Pck1* and *G6pc* expression (Yin et al., 2007). We speculate that decreased availability of heme, either from iron deficiency in skeletal muscle or liver, de-repressed expression of these gluconeogenic enzymes. However, in spite of their increased expression, Tfr1-null mice developed progressive hypoglycemia, indicating that gluconeogenesis failed. This is likely attributable to lack of substrate, as amino acids were profoundly decreased in muscle, serum and liver.

Even before steatosis developed, the liver showed profound downregulation of a large number of genes with various roles in the cell cycle, most of which are annotated as E2f targets. We are not certain why we see this striking pattern, but we note that Txnip, which is highly expressed in mutant muscle and liver, has been shown to cause cell cycle arrest (Han et al., 2003).

Severe iron deficiency in skeletal muscle compromises production of Fe–S clusters important for ETC complexes and other enzymes. However, our Tfr1-null muscle differed from muscle from human patients with Fe–S cluster depletion due to deficiency of the Fe–S cluster scaffold protein ISCU (Crooks et al., 2014). Similar to our mice, those patients had decreased mitochondrial aconitase activity, as expected. There were some similarities in gene expression but they were modest, and muscle mRNA expression of several key genes, including *TST*, *ALAS1* and *SLC25A28* was increased in the human patients, while expression of those genes or close homologs (*Tst*, *Alas2*, *Slc25a37*) was strongly decreased in muscle in our mice. Crooks et al. observed that fibroblast growth factor 21 (*FGF21*) mRNA was markedly induced in muscle samples from affected patients, but *Fgf21* was not induced in muscle from our mice (not shown). Furthermore, the patients were not reported to have hepatic steatosis or hypoglycemia. These differences suggest that loss of Tfr1 in skeletal muscle has consequences beyond depletion of Fe–S clusters and the proteins that require them.

The pattern of increased lysine acetylation we observed by proteomic analysis of Tfr1-null skeletal muscle was striking in two ways. First, nearly all hyperacetylated proteins were mitochondrial and most hypoacetylated proteins were not. Second, there was strong concordance between acetylation events we observed and those observed in Sirt3 −/− muscle. Both observations suggest that Sirt3 may be less active in Tfr1-null muscle, though we cannot exclude the possibility that increased mitochondrial acetyl CoA resulting from decreased mitochondrial aconitase activity, or increased acetylase activity, contributed to this pattern. It is possible that mitochondrial dysfunction has led to a deficit in acetyl donors outside of the mitochondria.

Surprisingly, iron deficiency in skeletal muscle also led to iron deficiency in the liver before the systemic phenotype was apparent. This seems counterintuitive – one might expect that a decrease in the ability of the muscle to extract iron from circulating Tf might lead to increased hepatic iron stores, but that was not what we observed. There are several possible explanations. First, muscle iron deficiency might instigate an as yet unidentified signal to the liver to decrease expression of the iron regulatory hormone hepcidin and mobilize hepatic iron stores. A similar signal has been described from the erythroid bone marrow to regulate intestinal iron absorption (Finch, 1994), apparently by decreasing hepcidin expression (Hentze et al., 2004). It was recently reported that erythroferrone (Fam132b) might be a component of this "erythroid regulator" (Kautz et al., 2014). Expression of erythroferrone was not increased in $Tfr1^{mu/mu}$ muscle (not shown), even though this protein has also been identified as myonectin and described as linking muscle activity to adipose tissue and liver lipid metabolism (Seldin et al., 2012). Alternatively, metabolic changes associated with iron deficiency in $Tfr1^{mu/mu}$ muscle might alter hepatic iron homeostasis in a manner not yet described. Regardless of the mechanism, decreased expression of the iron regulatory hormone hepcidin should result in increased iron availability to skeletal muscle. However, our results indicate that this is futile when Tfr1 is inactive in muscle.

Our experiments have allowed us to examine the local and systemic sequelae of severe, isolated muscle iron deficiency. While impairment of iron-dependent enzymes in muscle might have been predicted, the systemic effects are profound and surprising, and elucidate a previously unappreciated link between iron homeostasis and intermediary metabolism. We have studied an extreme situation, contrived by targeted disruption of Tfr1, but we speculate that less severe muscle iron deficiency may have hitherto unappreciated effects on systemic energy homeostasis. This could be quite significant clinically, as iron deficiency affects at least 15% of the world's population and is the third most prevalent cause of years lived with disability (Vos et al., 2012).

Author Contributions

TB and NCA designed the experiments and wrote the manuscript. TB carried out most of the experiments with the assistance from IL and MB. EJS and MAM carried out proteomic experiments and analyses. TRK and DMM performed metabolomics experiments and analyses.

Disclosures

NCA is a member of the Board of Directors of Novartis AG, but Novartis had no connection to the work described in this paper. There are no conflicts of interest to report.

Acknowledgments

We thank the Duke Microarray Shared Resource for microarray experiments and statistical analysis, John Shelton (UT Southwestern) for preparing muscle tissue sections, Ron Kahn, Brad Gibson and Matt Rardin for sharing unpublished data, Laura DuBois for preparing proteomics samples, Will Thompson for special contributions to the methodology used for acetylproteomics measurements and members of the Andrews laboratory for helpful discussions. Toby Eisenberg carried out related studies that provided insight into this project. EJS and MAM are faculty members in the Duke Proteomics and

Metabolomics Shared Resource. This work was supported by NIH R01 DK089705 to NCA and the Duke Microarray Shared Resource is partially supported by NIH P30 CA014236.

Appendix A. Supplementary data

Supplementary data to this article can be found online at http://dx.doi.org/10.1016/j.ebiom.2015.09.041.

References

An, J., Muoio, D.M., Shiota, M., Fujimoto, Y., Cline, G.W., Shulman, G.I., Koves, T.R., Stevens, R., Millington, D., Newgard, C.B., 2004. Hepatic expression of malonyl-CoA decarboxylase reverses muscle, liver and whole-animal insulin resistance. Nat. Med. 10, 268–274.

Anderson, K.A., Hirschey, M.D., 2012. Mitochondrial protein acetylation regulates metabolism. Essays Biochem. 52, 23–35.

Andrews, N.C., 1999. Medical Progress: Disorders of Iron Metabolism. N. Engl. J. Med. 341, 1986–1995.

Baker, E., Baker, S.M., Morgan, E.H., 1998. Characterisation of non-transferrin-bound iron (ferric citrate) uptake by rat hepatocytes in culture. Biochim. Biophys. Acta 1380, 21–30.

Barisani, D., Berg, C.L., Wessling-Resnick, M., Gollan, J.L., 1995. Evidence for a low Km transporter for non-transferrin-bound iron in isolated rat hepatocytes. Am. J. Phys. 269, G570–G576.

Barrientos, T., Andrews, N.C., 2015. Expression Data from Wildtype and Tfr1 Skeletal Muscle KO Mice. NCBI: NCBI Gene Expression Omnibus.

Bharathi, S.S., Zhang, Y., Mohsen, A.W., Uppala, R., Balasubramani, M., Schreiber, E., Uechi, G., Beck, M.E., Rardin, M.J., Vockley, J., Verdin, E., Gibson, B.W., Hirschey, M.D., Goetzman, E.S., 2013. Sirtuin 3 (SIRT3) protein regulates long-chain Acyl-CoA dehydrogenase by deacetylating conserved lysines near the active site. J. Biol. Chem. 288, 33837–33847.

Carson, F.L., Hladlik, C., 2009. Oil red O Method for Neutral Fats. In: Carson, F.L., Hladlik, C. (Eds.), *Histotechnology: A Self-Instructional Text*. American Society for Clinical Pathology Press, Chicago.

Chen, A.C., Donovan, A., Ned-Sykes, R., Andrews, N.C., 2015. A Non-Canonical Role of Transferrin Receptor 1 is Essential for Intestinal Homeostasis. Proc. Natl. Acad. Sci. U. S. A. 112, 11714–11719.

Courselaud, B., Pigeon, C., Inoue, Y., Inoue, J., Gonzalez, F.J., Leroyer, P., Gilot, D., Boudjema, K., Guguen-Guillouzo, C., Brissot, P., Loreal, O., Ilyin, G., 2002. C/EBPalpha regulates hepatic transcription of hepcidin, an antimicrobial peptide and regulator of iron metabolism. Cross-talk between C/EBP pathway and iron metabolism. J. Biol. Chem. 277, 41163–41170.

Crooks, D.R., Natarajan, T.G., Jeong, S.Y., Chen, C., Park, S.Y., Huang, H., Ghosh, M.C., Tong, W.H., Haller, R.G., Wu, C., Rouault, T.A., 2014. Elevated FGF21 secretion, PGC-1alpha and ketogenic enzyme expression are hallmarks of iron-sulfur cluster depletion in human skeletal muscle. Hum. Mol. Genet. 23, 24–39.

Finch, C., 1994. Regulators of iron balance in humans. Blood 84, 1697–1702.

Foster, D.B., Liu, T., Rucker, J., O'Meally, R.N., Devine, L.R., Cole, R.N., O'Rourke, B., 2013. The Cardiac Acetyl-Lysine Proteome. PLoS One 8, e67513.

Han, S.H., Jeon, J.H., Ju, H.R., Jung, U., Kim, K.Y., Yoo, H.S., Lee, Y.H., Song, K.S., Hwang, H.M., Na, Y.S., Yang, Y., Lee, K.N., Choi, I., 2003. VDUP1 upregulated by TGF-beta1 and 1,25-dihydorxyvitamin D3 inhibits tumor cell growth by blocking cell-cycle progression. Oncogene 22, 4035–4046.

Hentze, M.W., Muckenthaler, M.U., Andrews, N.C., 2004. Balancing acts: molecular control of mammalian iron metabolism. Cell 117, 285–297.

Jensen, M.V., Joseph, J.W., Ilkayeva, O., Burgess, S., Lu, D., Ronnebaum, S.M., Odegaard, M., Becker, T.C., Sherry, A.D., Newgard, C.B., 2006. Compensatory responses to pyruvate carboxylase suppression in islet beta-cells. Preservation of glucose-stimulated insulin secretion. J. Biol. Chem. 281, 22342–22351.

Kautz, L., JUNG, G., Valore, E.V., Rivella, S., Nemeth, E., Ganz, T., 2014. Identification of erythroferrone as an erythroid regulator of iron metabolism. Nat. Genet. 46, 678–684.

Kersten, S., Lichtenstein, L., Steenbergen, E., Mudde, K., Hendriks, H.F., Hesselink, M.K., Schrauwen, P., Muller, M., 2009. Caloric restriction and exercise increase plasma ANGPTL4 levels in humans via elevated free fatty acids. Arterioscler. Thromb. Vasc. Biol. 29, 969–974.

Kim, S.C., Sprung, R., Chen, Y., Xu, Y., Ball, H., Pei, J., Cheng, T., Kho, Y., Xiao, H., Xiao, L., Grishin, N.V., White, M., Yang, X.J., Zhao, Y., 2006. Substrate and functional diversity of lysine acetylation revealed by a proteomics survey. Mol. Cell 23, 607–618.

Klempa, K.L., Willis, W.T., Chengson, R., Dallman, P.R., Brooks, G.A., 1989. Iron deficiency decreases gluconeogenesis in isolated rat hepatocytes. J. Appl. Physiol. (1985) 67, 1868–1872.

Leonardi, R., Rehg, J.E., Rock, C.O., Jackowski, S., 2010. Pantothenate kinase 1 is required to support the metabolic transition from the fed to the fasted state. PLoS One 5, e11107.

Levy, J.E., Jin, O., Fujiwara, Y., Kuo, F., Andrews, N.C., 1999. Transferrin receptor is necessary for development of erythrocytes and the nervous system. Nat. Genet. 21, 396–399.

Li, J.Y., Paragas, N., Ned, R.M., Qiu, A., Viltard, M., Leete, T., Drexler, I.R., Chen, X., Sanna-Cherchi, S., Mohammed, F., Williams, D., Lin, C.S., Schmidt-Ott, K.M., Andrews, N.C., Barasch, J., 2009. Scara5 is a ferritin receptor mediating non-transferrin iron delivery. Dev. Cell 16, 35–46.

Liuzzi, J.P., Aydemir, F., Nam, H., Knutson, M.D., Cousins, R.J., 2006. Zip14 (Slc39a14) mediates non-transferrin-bound iron uptake into cells. Proc. Natl. Acad. Sci. U. S. A. 103, 13612–13617.

Miniou, P., Tiziano, D., Frugier, T., Roblot, N., Le Meur, M., Melki, J., 1999. Gene targeting restricted to mouse striated muscle lineage. Nucleic Acids Res. 27, e27.

Mohamed, J.S., Lopez, M.A., Cox, G.A., Boriek, A.M., 2013. Ankyrin repeat domain protein 2 and inhibitor of DNA binding 3 cooperatively inhibit myoblast differentiation by physical interaction. J. Biol. Chem. 288, 24560–24568.

Mootha, V.K., Lindgren, C.M., Eriksson, K.F., Subramanian, A., Sihag, S., Lehar, J., Puigserver, P., Carlsson, E., Ridderstrale, M., Laurila, E., Houstis, N., Daly, M.J., Patterson, N., Mesirov, J.P., Golub, T.R., Tamayo, P., Spiegelman, B., Lander, E.S., Hirschhorn, J.N., Altshuler, D., Groop, L.C., 2003. PGC-1alpha-responsive genes involved in oxidative phosphorylation are coordinately downregulated in human diabetes. Nat. Genet. 34, 267–273.

Muoio, D.M., 2007. TXNIP links redox circuitry to glucose control. Cell Metab. 5, 412–414.

Ned, R.M., Swat, W., Andrews, N.C., 2003. Transferrin receptor 1 is differentially required in lymphocyte development. Blood 102, 3711–3718.

Oudit, G.Y., Sun, H., Trivieri, M.G., Koch, S.E., Dawood, F., Ackerley, C., Yazdanpanah, M., Wilson, G.J., Schwartz, A., Liu, P.P., Backx, P.H., 2003. L-type Ca(2+) channels provide a major pathway for iron entry into cardiomyocytes in iron-overload cardiomyopathy. Nat. Med. 9, 1187–1194.

Ozden, O., Park, S.H., Wagner, B.A., Yong Song, H., Zhu, Y., Vassilopoulos, A., Jung, B., Buettner, G.R., Gius, D., 2014. SIRT3 deacetylates and increases pyruvate dehydrogenase activity in cancer cells. Free Radic. Biol. Med. 76, 163–172.

Pashkov, V., Huang, J., Parameswara, V.K., Kedzierski, W., Kurrasch, D.M., Tall, G.G., Esser, V., Gerard, R.D., Uyeda, K., Towle, H.C., Wilkie, T.M., 2011. Regulator of G protein signaling (RGS16) inhibits hepatic fatty acid oxidation in a carbohydrate response element-binding protein (ChREBP)-dependent manner. J. Biol. Chem. 286, 15116–15125.

Rardin, M.J., Newman, J.C., Held, J.M., Cusack, M.P., Sorensen, D.J., Li, B., Schilling, B., Mooney, S.D., Kahn, C.R., Verdin, E., Gibson, B.W., 2013. Label-free quantitative proteomics of the lysine acetylome in mitochondria identifies substrates of SIRT3 in metabolic pathways. Proc. Natl. Acad. Sci. U. S. A. 110, 6601–6606.

Rardin, M.J., Wiley, S.E., Naviaux, R.K., Murphy, A.N., Dixon, J.E., 2009. Monitoring phosphorylation of the pyruvate dehydrogenase complex. Anal. Biochem. 389, 157–164.

Rensvold, J.W., Ong, S.E., Jeevananthan, A., Carr, S.A., Mootha, V.K., Pagliarini, D.J., 2013. Complementary RNA and protein profiling identifies iron as a key regulator of mitochondrial biogenesis. Cell Rep. 3, 237–245.

Seldin, M.M., Peterson, J.M., Byerly, M.S., Wei, Z., Wong, G.W., 2012. Myonectin (CTRP15), a novel myokine that links skeletal muscle to systemic lipid homeostasis. J. Biol. Chem. 287, 11968–11980.

Spinazzi, M., Casarin, A., Pertegato, V., Ermani, M., Salviati, L., Angelini, C., 2011. Optimization of respiratory chain enzymatic assays in muscle for the diagnosis of mitochondrial disorders. Mitochondrion 11, 893–904.

Sturrock, A., Alexander, J., Lamb, J., Craven, C.M., Kaplan, J., 1990. Characterization of a transferrin-independent uptake system for iron in HeLa cells. J. Biol. Chem. 265, 3139–3145.

Subramanian, A., Tamayo, P., Mootha, V.K., Mukherjee, S., Ebert, B.L., Gillette, M.A., Paulovich, A., Pomeroy, S.L., Golub, T.R., Lander, E.S., Mesirov, J.P., 2005. Gene set enrichment analysis: a knowledge-based approach for interpreting genome-wide expression profiles. Proc. Natl. Acad. Sci. U. S. A. 102, 15545–15550.

Thyfault, J.P., Cree, M.G., Zheng, D., Zwetsloot, J.J., Tapscott, E.B., Koves, T.R., Ilkayeva, O., Wolfe, R.R., Muoio, D.M., Dohm, G.L., 2007. Contraction of insulin-resistant muscle normalizes insulin action in association with increased mitochondrial activity and fatty acid catabolism. Am. J. Physiol. Cell Physiol. 292, C729–C739.

Trenor III, C.C., Campagna, D.R., Sellers, V.M., Andrews, N.C., Fleming, M.D., 2000. The molecular defect in hypotransferrinemic mice. Blood 96, 1113–1118.

Truett, G.E., Heeger, P., Mynatt, R.L., Truett, A.A., Walker, J.A., Warman, M.L., 2000. Preparation of PCR-quality mouse genomic DNA with hot sodium hydroxide and tris (HotSHOT). Biotechniques 29 (52), 54.

Vos, T., Flaxman, A.D., Naghavi, M., Lozano, R., Michaud, C., Ezzati, M., Shibuya, K., Salomon, J.A., Abdalla, S., Aboyans, V., Abraham, J., Ackerman, I., Aggarwal, R., Ahn, S.Y., Ali, M.K., Alvarado, M., Anderson, H.R., Anderson, L.M., Andrews, K.G., Atkinson, C., Baddour, L.M., Bahalim, A.N., Barker-Collo, S., Barrero, L.H., Bartels, D.H., Basanez, M.G., Baxter, A., BELL, M.L., Benjamin, E.J., Bennett, D., Bernabe, E., Bhalla, K., Bhandari, B., Bikbov, B., Bin Abdulhak, A., Birbeck, G., Black, J.A., Blencowe, H., Blore, J.D., Blyth, F., Bolliger, I., Bonaventure, A., Boufous, S., Bourne, R., Boussinesq, M., Braithwaite, T., Brayne, C., Bridgett, L., Brooker, S., Brooks, P., Brugha, T.S., Bryan-Hancock, C., Bucello, C., Buchbinder, R., Buckle, G., Budke, C.M., Burch, M., Burney, P., Burstein, R., Calabria, B., Campbell, B., Canter, C.E., Carabin, H., Carapetis, J., Carmona, L., Cella, C., Charlson, F., Chen, H., Cheng, A.T., Chou, D., Chugh, S.S., Coffeng, L.E., Colan, S.D., Colquhoun, S., Colson, K.E., Condon, J., Connor, M.D., Cooper, L.T., Corriere, M., Cortinovis, M., De Vaccaro, K.C., Couser, W., Cowie, B.C., Criqui, M.H., Cross, M., Dabhadkar, K.C., Dahiya, M., Dahodwala, N., Damsere-Derry, J., Danaei, G., Davis, A., De Leo, D., Degenhardt, L., Dellavalle, R., Delossantos, A., Denenberg, J., Derrett, S., Des Jarlais, D.C., Dharmaratne, S.D., Dherani, M., et al., 2012. Years lived with disability (YLDs) for 1160 sequelae of 289 diseases and injuries 1990–2010: a systematic analysis for the global burden of disease study 2010. Lancet 380, 2163–2196.

Walden, W.E., Selezneva, A.I., Dupuy, J., Volbeda, A., Fontecilla-Camps, J.C., Theil, E.C., Volz, K., 2006. Structure of dual function iron regulatory protein 1 complexed with ferritin IRE-RNA. Science 314, 1903–1908.

Walsh, J.J., Edgett, B.A., Tschakovsky, M.E., Gurd, B.J., 2015. Fasting and exercise differentially regulate BDNF mRNA expression in human skeletal muscle. Appl. Physiol. Nutr. Metab. 40, 96–98.

Wang, N.D., Finegold, M.J., Bradley, A., Ou, C.N., Abdelsayed, S.V., Wilde, M.D., Taylor, L.R., Wilson, D.R., Darlington, G.J., 1995. Impaired energy homeostasis in C/EBP alpha knockout mice. Science 269, 1108–1112.

Wieckowski, M.R., Giorgi, C., Lebiedzinska, M., Duszynski, J., Pinton, P., 2009. Isolation of mitochondria-associated membranes and mitochondria from animal tissues and cells. Nat. Protoc. 4, 1582–1590.
Wu, J.Y., Kao, H.J., Li, S.C., Stevens, R., Hillman, S., Millington, D., Chen, Y.T., 2004. ENU mutagenesis identifies mice with mitochondrial branched-chain aminotransferase deficiency resembling human maple syrup urine disease. J. Clin. Invest. 113, 434–440.
Xu, W., Barrientos, T., Andrews, N.C., 2013. Iron and copper in mitochondrial diseases. Cell Metab. 17, 319–328.
Xu, A., Lam, M.C., Chan, K.W., Wang, Y., Zhang, J., Hoo, R.L., Xu, J.Y., Chen, B., Chow, W.S., Tso, A.W., Lam, K.S., 2005. Angiopoietin-like protein 4 decreases blood glucose and improves glucose tolerance but induces hyperlipidemia and hepatic steatosis in mice. Proc. Natl. Acad. Sci. U. S. A. 102, 6086–6091.
Yang, J., Goetz, D., Li, J.Y., Wang, W., Mori, K., Setlik, D., Du, T., Erdjument-Bromage, H., Tempst, P., Strong, R., Barasch, J., 2002. An iron delivery pathway mediated by a lipocalin. Mol. Cell 10, 1045–1056.
Yin, L., Wu, N., Curtin, J.C., Qatanani, M., Szwergold, N.R., Reid, R.A., Waitt, G.M., Parks, D.J., Pearce, K.H., Wisely, G.B., Lazar, M.A., 2007. Rev-Erbalpha, a heme sensor that coordinates metabolic and circadian pathways. Science 318, 1786–1789.